http://doi.org/10.35784/iapgos.3247 received: 6.11.2022 | revised: 11.12.2022 | accepted: 15.12.2022 | available online: 30.12.2022

POLARIZATION TOMOGRAPHY OF THE POLYCRYSTALINNE STRUCTURE OF HISTOLOGICAL SECTIONS OF HUMAN ORGANS IN DETERMINATION OF THE OLD DAMAGE

Olexandra Litvinenko[1], Victor Paliy[2], Olena Vysotska[3], Inna Vishtak[4], Saule Kumargazhanova[5]
[1]Higher State Educational Institution of Ukraine „Bukovynian State Medical University", Chernivtsi, Ukraine, [2]National Aerospace University H.E. Zhukovsky „Kharkiv Aviation Institute", Kharkiv, Ukraine, [3]National Pirogov Memorial University of Vinnytsia, Vinnytsia, Ukraine, [4]Vinnytsia National Technical University, Vinnytsia, Ukraine, [5]D. Serikbayev East Kazakhstan Technical University, Ust-Kamenogorsk, Kazakhstan

Abstract. *The results of algorithmic approbation of the technique of polarization tomography digital histological study of the age of damage to the myocardium and lung tissue based on the polarization reconstruction of linear birefringence maps are presented. Relationships between the temporal change in the magnitude of statistical moments of 1-4 orders characterizing the distribution of the magnitude of the degree of crystallization of histological sections of the myocardium and lung tissue and the duration of damage were determined. Established time intervals and accuracy of determining the prescription of damage to the myocardium and lung tissue.*

Keywords: polarization, tomography, optical anisotropy, biological tissues

TOMOGRAFIA POLARYZACYJNA STRUKTURY POLIKRYSTALICZNEJ WYCINKÓW HISTOLOGICZNYCH NARZĄDÓW CZŁOWIEKA W OKREŚLANIU DAWNYCH USZKODZEŃ

Streszczenie. *Przedstawiono wyniki algorytmicznej aprobaty techniki polaryzacyjnej tomografii cyfrowej histologicznego badania wieku uszkodzenia mięśnia sercowego i tkanki płucnej na podstawie rekonstrukcji polaryzacyjnej liniowych map dwójłomności. Określono zależności pomiędzy czasową zmianą wartości momentów statystycznych 1-4 rzędów, charakteryzujących rozkład stopnia krystalizacji skrawków histologicznych tkanki mięśnia sercowego i płuc, a czasem trwania uszkodzeń. Ustalono przedziały czasowe i dokładność określania predykcji uszkodzenia mięśnia sercowego i tkanki płucnej.*

Słowa kluczowe: polaryzacja, tomografia, anizotropia optyczna, tkanki biologiczne

Introduction

Histological study of microscopic images at different optical scales of the morphological structure of biological preparations is currently considered in the approximation of an objective (statistical) analysis of the distributions of photometric and polarization parameters [6, 12].

This approach makes it possible to determine a set of diagnostic relationships between a set of statistical moments of the 1st – 4th orders characterizing the distribution of structural anisotropy parameters of the morphological structure of the histological sections of biological tissues and two-dimensional distributions (polarization maps) of the magnitude of the azimuths and polarization ellipticity of their microscopic images [7, 14].

This work is aimed at further research and substantiation of new information possibilities of forensic digital histological examination using the method of polarization-phase tomography of birefringence distributions of histological sections of the myocardium and lung tissue in the problem of determining the age of damage [1, 8, 15].

1. Study design

The design of polarization tomography of the polycrystalline structure of histological sections of biological tissues of human internal organs is illustrated by the structural and logical scheme shown in table 1.

Table 1. Styles predefined in IAPGOS template

Structural-logical scheme of polarization tomography
Laser probe shaping unit
Block of multichannel formation of polarization probes
Block for placement of the studied histological section
Block for designing microscopic images of different scales
Block of multichannel polarization filtering of microscopic images
Block for digital registration of polarization filtered microscopic images
Block of algorithmic calculation of maps of linear and circular birefringence

2. Short theory and method

The structural and logical scheme of the Mueller-matrix tomography of histological sections of biological tissues contains:

I – optical sounding unit containing a source of coherent radiation – He-Ne laser [9, 11, 12];

II – block for forming an optical probe with a flat wavefront – two confocality located microobjectives with a vignette diaphragm.;

III – block for forming discrete states of polarization of the optical probe – phase-shifting plates 0.25λ and a linear polarizer that provide the formation of three types of linear polarization ($\alpha_0 = 0°;\ 90°;\ 45°$), as well as right circularly ($\otimes$) polarized laser radiation;

IV – object block – a microscopic table with a mount, adjustment and rotation of a biological sample;

V – projection unit – a polarizing microlens that provides the formation of a microscopic image of a biological preparation in the plane of a digital camera;

VI – polarization analysis block - phase-shifting plates 0.25λ and a linear polarizer, providing polarization analysis of the microscopic image of the biological layer 8 according to the following algorithm $\Omega = 0°; 90°; 45°; 135°; \otimes; \oplus$;

VII – block for digital registration of coordinate distributions of the intensity of polarization images of biological samples – a digital camera with $m \times n$ – the number of pixels of the photosensitive area;

VIII – block of analytical information processing – a personal computer and a package of applied programs that provide the calculation of the coordinate distributions of the parameters of the phase ($\delta_{0,90};\ \delta_{45,135};\ \delta_{\otimes,\otimes}$) and amplitude ($\Delta\mu_{0,90};\ \Delta\mu_{45,135};\ \Delta\mu_{\otimes,\otimes}$) anisotropy of partially depolarizing biological layers.

Optical probing of histological sections (polycrystalline films) of biological preparations was carried out using a beam of a gas He-Ne laser 1 formed by a collimator, parallel with a diameter of 2 mm, with a wavelength of λ = 0.6328 μm.

The formation of discrete states of polarization of the optical probe was carried out using phase-shifting (0.25λ) plates (manufacturer – Achromatic True Zero-Order Waveplate) and a dichroic polarizer 4 (manufacturer – B+W Kaesemann XS-ProPolarizer MRC Nano). The biological layer was sequentially probed with a laser beam with the following types of polarization: linear with azimuths of 0°, 90°, +45° and right-handed circulation (⊗). The formation of a series of linear states of polarization was carried out by orienting the axis of the highest velocity of the phase-shifting element 3 at an angle of ÷ 45° relative to the plane of polarization of laser radiation, followed by rotation of the plane of transmission of the polarizer at angles of 0°, 90°, +45°. A right circularly polarized wave was formed by introducing a phase-shifting quarter-waveplate with the axis of maximum velocity oriented at an angle of 0° relative to the plane of polarization of the laser beam +45°. Laser radiation intensity distributions in the plane of histological sections (polycrystalline films) of biological preparations were formed using a polarizing microlens (manufacturer – Nikon CFI Achromatic P, focal length – 30 mm, numerical aperture – 0.1, magnification – 4x) (The Imaging Source DMK 41AU02.AS, monochrome 1/2" CCD, Sony ICX205AL (progressive scan); resolution – 1280×960; size of the light-sensitive area – 7600×6200 μm; sensitivity – 0.05 lx; dynamic range of which are a contains m×n = 1280×960 pixels.

Polarization filtering of the coordinate distributions of the intensity of microscopic images of histological sections (polycrystalline films) of biological preparations was carried out using a linear polarizer (the transmission plane angle was the following discrete values $0°;\ 90°;\ 45°; 135°$) and a quarter-wave phase plate 8 (the orientation angle of the axis of maximum velocity was $45°; 135°$) [9, 10, 11].

The data obtained make it possible to determine expressions for calculating the optical anisotropy parameters characterizing the linear and circular:

- birefringence ($LB_{0.90};\ \ LB_{45.135};\ \ CB_{\otimes,\oplus}$):

$$\left.\begin{aligned}\langle m_{34}\rangle &= r^{-1}\,ln\left(\frac{f_{34}}{f_{43}}\right) = r^{-1}\,ln\left(\frac{S_3^{\otimes}-0.5(S_3^0+S_3^{90})}{S_4^{45}-0.5(S_4^0+S_4^{90})}\right)\\ \langle m_{34}\rangle &= r^{-1}\,ln\left(\frac{f_{43}}{f_{34}}\right) = r^{-1}\,ln\left(\frac{S_4^{45}-0.5(S_4^0+S_4^{90})}{S_3^{\otimes}-0.5(S_3^0+S_3^{90})}\right)\end{aligned}\right\} \Rightarrow LB_{0.90} \quad (1)$$

$$\left.\begin{aligned}\langle m_{42}\rangle &= r^{-1}\,ln\left(\frac{f_{42}}{f_{24}}\right) = r^{-1}\,ln\left(\frac{0.5(S_4^0-S_4^{90})}{S_2^{\otimes}-0.5(S_2^0+S_2^{90})}\right)\\ \langle m_{24}\rangle &= r^{-1}\,ln\left(\frac{f_{24}}{f_{42}}\right) = r^{-1}\,ln\left(\frac{S_2^{\otimes}-0{,}5(S_2^0+S_2^{90})}{0.5(S_4^0-S_4^{90})}\right)\end{aligned}\right\} \Rightarrow LB_{45.135} \quad (2)$$

$$\left.\begin{aligned}\langle m_{23}\rangle &= r^{-1}\,ln\left(\frac{f_{23}}{f_{32}}\right) = r^{-1}\,ln\left(\frac{S_2^{45}-0.5(S_2^0+S_2^{90})}{0.5(S_3^0-S_3^{90})}\right)\\ \langle m_{32}\rangle &= r^{-1}\,ln\left(\frac{f_{32}}{f_{23}}\right) = r^{-1}\,ln\left(\frac{0.5(S_3^0-S_3^{90})}{S_2^{45}-0.5(S_2^0+S_2^{90})}\right)\end{aligned}\right\} \Rightarrow CB_{\otimes,\oplus} \quad (3)$$

- dichroism ($LD_{0.90}\quad LD_{45.135}\quad CD_{\otimes,\oplus}$):

$$\langle m_{12}\rangle = \langle m_{21}\rangle = r^{-1}\,ln(f_{12}f_{21}) = $$
$$= r^{-1}\,ln\left(0.25(S_1^0 - S_1^{90})(S_2^0 + S_2^{90})\right) \Rightarrow LD_{0.90} \quad (4)$$

$$\langle m_{13}\rangle = \langle m_{31}\rangle = r^{-1}\,ln(f_{13}f_{31}) = $$
$$= r^{-1}\,ln\left(0.25\left(S_1^{45} - 0.5(S_1^0 + S_1^{90})\right)(S_3^0 + S_3^{90})\right) \Rightarrow$$
$$\Rightarrow LD_{45.135} \quad (5)$$

$$\langle m_{14}\rangle = \langle m_{41}\rangle = r^{-1}\,ln(f_{14}f_{41}) = $$
$$= r^{-1}\,ln\left(0.25\left(S_1^{\otimes} - 0.5(S_1^0 + S_1^{90})\right)(S_4^0 + S_4^{90})\right) \Rightarrow$$
$$\Rightarrow CD_{\otimes,\oplus}. \quad (6)$$

Here $S_{i=2;3;4}^{0;45;90;\otimes}$ – set of parameters of the Stokes vector at the points of a digital microscopic image of a sample of a partially depolarizing biological layer, experimentally determined for a series of linearly ($0^0;\ 45^0;\ 90^0$) and right-circular (⊗) polarized probing laser beams according to the following relations

$$S_{i=1}^{0;45;90;\otimes} = I_0^{0;45;90;\otimes} + I_{90}^{0;45;90;\otimes};$$
$$S_{i=2}^{0;45;90;\otimes} = I_0^{0;45;90;\otimes} - I_{90}^{0;45;90;\otimes};$$
$$S_{i=3}^{0;45;90;\otimes} = I_{45}^{0;45;90;\otimes} - I_{135}^{0;45;90;\otimes};$$
$$S_{i=4}^{0;45;90;\otimes} = I_{\otimes}^{0;45;90;\otimes} + I_{\oplus}^{0;45;90;\otimes} \quad (7)$$

Here $I_{0;45;90;135;\otimes;\oplus}$ – polarization-filtered intensities of laser radiation converted by a biological object. The filtering operation corresponds to the following experimental actions – the passage of an object beam through a linear polarizer 9 with the angles of rotation of the transmission axis Θ: $0^0;\ \ 45^0;\ \ 90^0;\ \ 135^0$, as well as through the phase filtering system „quarter-waveplate – polarizer", which separates the right – (⊗) and left – (⊕) circularly polarized components of the object laser radiation [2, 3, 10].

3. Algorithm for determining the prescription of the formation of damage to the internal organs of a person

The criterion for detecting the interval for determining the prescription of damage formation is the time interval (τ) of a continuous linear change in the magnitude of the statistical moments of the 1st – 4th moments ($Z_{i\,=\,1;2;3;4}$), characterizing the distribution of optical-anisotropic parameters (birefringence, LB) histological sections, which provides an analysis of the morphological structure of various biological tissues [4, 5, 10].

The scheme of algorithmic determination of the prescription of damage to internal organs is shown in Fig. 1.

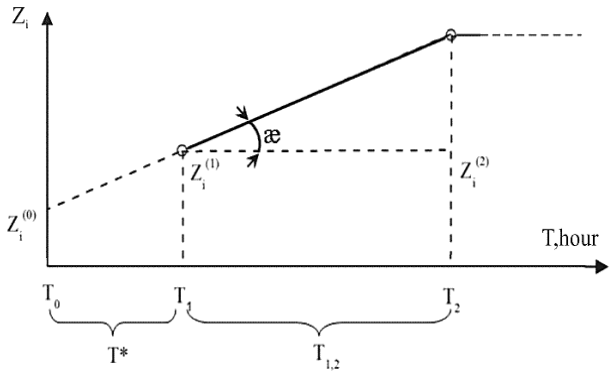

Fig. 1. Scheme of algorithmic determination of damage age: τ_1 – time of the beginning of measurements of the magnitude of statistical moments of the 1st – 4th orders $Z_i^{(1)}$; τ_2 – completion time of the linear change in the magnitude of statistical moments of the 1st – 4th orders $Z_i^{(2)}$; τ_0 – unknown time of occurrence of damage; ϰ – time dependence slope $Z_i^{(τ)}$

An analysis of the algorithmic scheme (Fig. 1) revealed the following relationships for determining the prescription (time τ^*) of damage to human internal organs with an accuracy $\Delta\tau^*$

$$\tau^* = \left(Z_i^{(1)} - Z_i^{(0)}\right)\frac{\tau_2-\tau_1}{Z_i^{(2)}-Z_i^{(1)}} \quad (8)$$

Here $Z_i^{(0)}$ is the value of the statistical moment calculated for the polarization-tomographic map of linear birefringence LB of the histological section of intact biological tissue [1, 8, 13].

4. Analysis and discussion of experimental data

4.1. Myocardium

The following groups were formed (control of those who died from coronary heart disease (CHD)) and experimental (with different duration of damage τ^*) samples of histological sections of the human myocardium and lung tissue – table 2.

Table 2. Characteristics of the objects of study

Groups									
Control	Experienced with different prescription damage, hours								
Died from CHD	1	6	12	18	24	48	72	96	120
(number of samples *n = 21*)	*n = 21*	*n = 21*	*n = 21*	*n = 21*	*n = 21*	*n = 21*	*n = 21*	*n = 21*	*n = 21*

Within each of the groups of histological sections:

- maps of linear birefringence were determined LB,
- statistical moments of the 1st – 4th orders ($Z_{i=1,2,3,4}$), characterizing the distribution of the quantity LB was calculated,
- was determined within the framework of the control and the totality of experimental groups, the average value and the error of the value of each of the statistical moments of 1–4 orders,
- algorithmically (formula (1)) the age of damage was calculated – τ^*.

Fig. 2 shows the coordinate distributions ((1) – (3)) of the magnitude of linear birefringence (LB) of histological sections of the myocardium of the dead from the control group (1), experimental groups with different duration of damage (6 hours – (2)) and (18 hours – (3)).

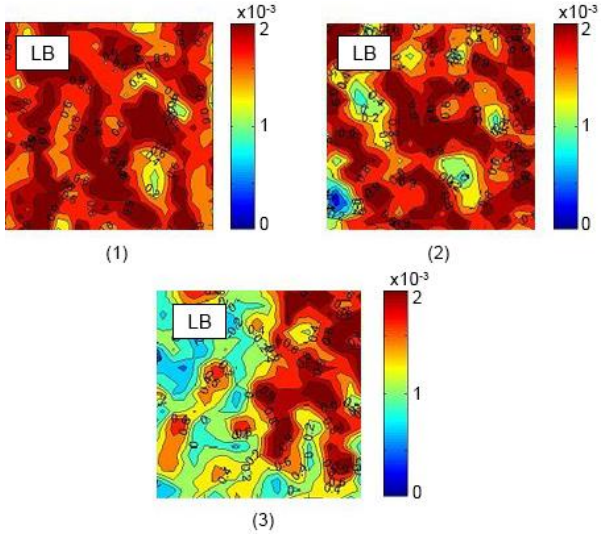

Fig. 2. Coordinate distributions ((1)–(3)) of the linear birefringence of histological sections of the myocardium of the dead from the control group ((1)), research groups with different damage duration (6 hours – (2)) and (18 hours – (3))

Table 3. Time dynamics of changes in statistical moments of 1–4 orders characterizing the distribution of the magnitude of linear birefringence (LB) of histological sections of the myocardium

***T*, hours**	**2**	**4**	**6**	**12**	**18**
$Z_1 \times 10^{-1}$	1.74±0.069	1.54±0.058	1.34±0.057	1.12±0.049	0.93±0.038
p	$p < 0.05$				
$Z_2 \times 10^{-1}$	1.29±0.055	0.97±0.039	0.64±0.028	0.41±0.019	0.38±0.018
p	$p < 0.05$				$p > 0.05$
Z_3	0.38±0.016	0.54±0.023	0.71±0.035	1.24±0.056	1.53±0.069
p	$p < 0.05$				
Z_4	0.25±0.011	0.49±0.022	0.73±0.034	1.21±0.056	1.69±0.069
p	$p < 0.05$				
***T*, hours**	**24**	**48**	**72**	**96**	**120**
$Z_1 \times 10^{-1}$	0.73±0.035	0.51±0.022	0.52±0.021	0.49±0,022	0.48±0.021
p	$p < 0.05$		$p > 0.05$		
$Z_2 \times 10^{-1}$	0.38±0.017	0.35±0.016	0.33±0.017	0.34±0,018	0.33±0.016
p	$p < 0.05$	$p > 0.05$			
Z_3	1.65±0.071	2.01±0.092	2.36±0.105	2.29±0,11	2.28±0.12
p	$p < 0.05$			$p > 0.05$	
Z_4	2.02±0.099	2.59±0.12	3.07±0.14	3.13±0.15	3.09±0.14
p	$p < 0.05$			$p > 0.05$	

From the analysis of the data obtained, it can be seen:

- histological sections of the myocardium of the dead from all the studied groups have linear birefringence – LB ≠ 0,
- with an increase in the time of damage, the average level and the root-mean-square spread of random values of the linear birefringence value decrease LB.

Table 2 illustrates the time dependences of the set of statistical moments of 1–4 orders characterizing the coordinate distributions of the LB value of histological sections of the myocardium of the dead.

Dynamic ranges were established, as well as diagnostic sensitivity to the prescription of myocardial damage of statistical moments of the 1st–4th orders ($Z_{i=1;2;3;4}$) with subsequent linear time intervals (highlighted in color – table 1; $\propto$ = const – Fig.1) and a statistically significant change ($p \leq 0.05$) of the Eigen values of the linear birefringence LB:

- 1st order statistical moment (average Z_1) – 48 hours and 1.23,
- 2nd order statistical moment (dispersionZ_2) – 24 hours and 0.91,
- 3rd order statistical moment (asymmetryZ_3) – 72 hours and 1.98,
- 4th order statistical moment (kurtosis Z_4) – 72 hours and 2.82.

4.2. Lung tissue

The results of a digital histological study of the degree of crystallization of lung tissue samples from the experimental (1) and two control (2), (3) groups are shown in Fig. 3.

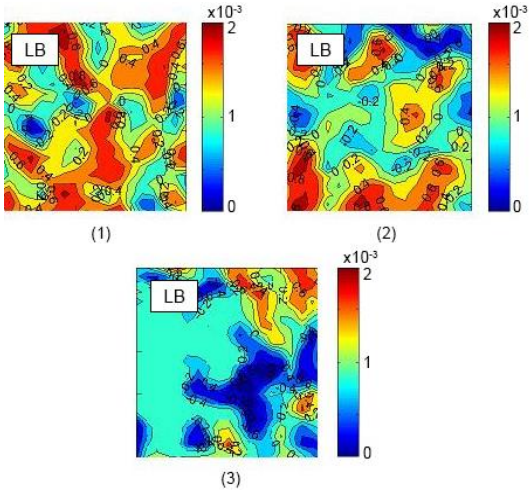

Fig. 3. Coordinate distributions ((1)–(3)) of the linear birefringence of histological sections of the lung tissue of the dead from the control group ((1)), research groups with different damage duration (6 hours – (2)) and (18 hours – (3))

As in the case of a polarization tomographic study of myocardial samples, for the obtained data on the optical anisotropy of lung tissue samples, one can see:

- histological sections of the lung tissue of the deceased from all the studied groups have linear birefringence – LB ≠ 0,
- the average level and spread of the LB value is 1.2 – 2 times less than the similar parameter of the optical anisotropy of the myocardium,
- with an increase in the time of damage, the average level and the root-mean-square spread of random values of the linear birefringence value decrease LB.

Table 4. Time dynamics of changes in statistical moments of 1–4 orders characterizing the distribution of the magnitude of linear birefringence (LB) of histological sections of the lung tissue

***T*, hours**	**2**	**4**	**6**	**12**	**18**
$Z_1 \times 10^{-1}$	0.58±0.024	0.53±0.021	0.48±0.029	0.38±0.017	0.28±0.015
p	p < 0.05				
$Z_2 \times 10^{-1}$	0.39±0.019	0.33±0.013	0.27±0.014	0.21±0.014	0.15±0.007
p	p < 0.05				
Z_3	1.43±0.065	1.64±0.077	1.83±0.081	2.11±0.099	2.44±0.11
p	p < 0,05				
Z_4	1.77±0.073	2.01±0.098	2.19±0.105	2.68±0.12	3.21±0.14
p	p < 0.05				
***T*, hours**	**24**	**48**	**72**	**96**	**120**
$Z_1 \times 10^{-1}$	0.18±0.008	0.13±0.006	0.12±0.007	0.13±0.008	0.12±0.007
p	p < 0.05		p > 0.05		
$Z_2 \times 10^{-1}$	0.12±0.005	0.15±0.008	0.13±0.007	0.14±0.008	0.13±0.007
p	p < 0.05	p > 0,05			
Z_3	2.82±0.13	3.19±0.15	3.57±0.16	3.45±0.16	3.49±0.17
p	p < 0.05			p > 0.05	
Z_4	3.63±0.17	4.06±0.19	4.78±0.21	4.66±0.21	4.77±0.21
p	p < 0.05			p > 0.05	

The revealed differences between the maps of linear birefringence of the myocardium and lung tissue can be attributed to the fact that the cardiac muscle is formed by spatially structured networks of myosin fibrils, which form a significantly higher level of structural anisotropy compared to the parenchyma structure of lung tissue.

Table 4 illustrates the time dependences of the value of the set of statistical moments of 1-4 orders, characterizing the distribution of the LB value of histological sections of the lung tissue of the dead.

From the analysis of data from digital polarization tomographic histology of lung tissue samples from the control group and experimental groups with different duration of damage, the following diagnostically relevant linear time intervals and ranges of changes in the magnitude of statistical moments of 1–4 orders of magnitude were established:

- 1st order statistical moment (average Z_1) – 48 hours and 0.45,
- 2nd order statistical moment (dispersion Z_2) – 24 hours and 0.27,
- 3rd order statistical moment (asymmetry Z_3) – 72 hours and 2.14,
- 4th order statistical moment (kurtosis Z_4) – 72 hours and 3.01.

5. Time intervals and accuracy of digital histological determination of damage age by polarization tomography

The time intervals and accuracy of determining the prescription of damage to the myocardium and lung tissue by the method of polarization tomography digital histology are presented in table 5.

Table 5. Time intervals and accuracy of the polarization mapping method for linear birefringence maps

Samples	Myocardium		Lung tissue	
Statistical moments	Interval, hours	Accuracy, min.	Interval, hours	Accuracy, min.
Average	1–48	35	1–48	45
Dispersion	1–24	35	1–24	45
Asymmetry	1–72	25	1–72	35
Kurtosis	1–72	25	1–72	35

6. Conclusions

1. The main interrelations between temporal changes in the statistical structure of topographic maps of the degree of crystallization of histological sections of the myocardium and lung tissue and variations in the magnitude of statistical moments of 1–4 orders that characterize them are revealed.
2. The time ranges of linear changes in the magnitude of statistical indicators of the tomography technique of digital histology and the accuracy of determining the age of damage were established:

- average, dispersion – 24–48 hours, accuracy 35 min. – 45 min.,
- asymmetry, kurtosis – 72 hours, accuracy 25 min. – 35 min.

References

[1] Avrunin, O. G. et al.: Possibilities of automated diagnostics of odontogenic sinusitis according to the computer tomography data. Sensors 21(4), 2021, 1–22.
[2] Blatter C. et al.: Dove prism based rotating dual beam bidirectional Doppler oct. Biomed. Opt. Express 4, 2013, 1188–1203.
[3] Hong Y.-J. et al.: Optically buffered Jones-matrix-based multifunctional optical coherence tomography with polarization mode dispersion correction. Biomed. Opt. Express 1, 2015, 225–243.
[4] Isaieva O. A. et al.: Features of image analysis under UV-video dermoscopy. Proc. of SPIE 11456, 2020, 114560H.
[5] Kovalova A. et al.: Possibilities of automated image processing at optical capillaroscopy. Proc. of SPIE 11456, 2020, 114560G.
[6] Macdonald C., Meglinski I.: Backscattering of circular polarized light from a disperse random medium influenced by optical clearing. Laser Phys. Lett. 8(4), 2011, 324–328.
[7] Park B. H., de Boer J. F.: Polarization sensitive optical coherence tomography. In: Drexler W., Fujimoto J. G. (Eds.): Optical Coherence Tomography: Technology and Applications, 2nd ed. Springer Reference, Science + Business Media, New York 2015, 1055–1101.
[8] Peyvasteh M., Tryfonyuk L. et al.: 3D Mueller-matrix-based azimuthal invariant tomography of polycrystalline structure within benign and malignant soft-tissue tumours. Laser Physics Letters 17(11), 2020, 115606.
[9] Rovira J. R. et al.: Methods and resources for imaging polarimetry. Proc. of SPIE 8698, 2012, 86980T.
[10] Ushenko V. A. et al.: 3D Mueller matrix mapping of layered distributions of depolarisation degree for analysis of prostate adenoma and carcinoma diffuse tissues. Scientific Reports 11(1), 2021, 5162.
[11] Ushenko V. A. et al.: Embossed topographic depolarisation maps of biological tissues with different morphological structures. Scientific Reports 11(1), 2021, 3871.
[12] Wang W. et al.: Roles of linear and circular polarization properties and effect of wavelength choice on differentiation between ex vivo normal and cancerous gastric samples. J. Biomed. Opt. 19(4), 2014, 046020.
[13] Wójcik W. et al.: Information Technology in Medical Diagnostics II. Taylor & Francis Group, CRC Press, Balkema book, London 2019.
[14] Yamanari M. et al.: Scleral birefringence as measured by polarizationsensitive optical coherence tomography and ocular biometric parameters of human eyes in vivo. Biomed. Opt. Express 5(5), 2014, 1391–1402.
[15] Yasuno Y. et al.: Jones Matrix based polarization sensitive optical coherence tomography. In: Drexler W., Fujimoto J. G. (Eds.): Optical Coherence Tomography: Technology and Applications, 2nd ed. Springer Reference, Science + Business Media, New York 2015, 1137–1162.

M.Sc. Olexandra Litvinenko
e-mail: sawasawa901@gmail.com

Postgraduate student at the Department of Forensic Medicine and Medical Law, Bukovina State Medical University, Ukraine. Research interests: digital and polarisation histology of biological tissues in the tasks of damage type and time detection.

http://orcid.org/0000-0003-3897-6765

D.Sc. Victor Paliy
e-mail: paliy@vnmu.edu.ua

Doctor of medical sciences, professor at the Department of General Surgery, National Pirogov Memorial University of Vinnytsia.
Scientific direction – research of antimicrobial efficacy of a medicines with prolonged antiseptic effect and their use for treatment of purulent wounds.

http://orcid.org/0000-0002-2289-1786

D.Sc. Olena Vysotska
e-mail: evisotska@ukr.net

Head of Department of Radio-electronic and Biomedical Computer-aided Means and Technologies National Aerospace University H.E. Zhukovsky "Kharkiv Aviation Institute", Ukraine.
Scientific direction – medical expert systems, modeling in medicine, proceeding of biomedical imaging and signals.

http://orcid.org/0000-0003-3723-9771

Ph.D. Inna Vishtak
e-mail: vishtakiv@vntu.edu.ua

Candidate of technical sciences, assistant professor. Assistant of the Department Safety of Life and Safety's Pedagogy, Deputy Director of the Institute of Doctoral and Postgraduate Studies, Vinnytsia National Technical University.
Scientific direction – mechatronics, mechanics, biomechanics and nanosructures, life safety, labor protection. Expert of the National Agency for Quality Assurance of Higher Education.

http://orcid.org/0000-0001-5646-4996

Ph.D. Saule Kumargazhanova
e-mail: SKumargazhanova@gmail.com

She is currently the Dean of the Department of Information Technologies and Intelligent Systems of D. Serikbayev East Kazakhstan Technical University. Author over 50 papers in journals and conference proceedings. Her professional interests are software engineering, data processing and analysis.

http://orcid.org/0000-0002-6744-4023